The Polar Transition from Alpha to Beta Regions Set by a Surface Buoyancy Flux Inversion

Romain Caneill, Fabien Roquet, Gurvan Madec, Jonas Nycander

The Polar Transition from Alpha to Beta Regions Set by a Surface Buoyancy Flux Inversion

ROMAIN CANEILL,[a] FABIEN ROQUET,[a] GURVAN MADEC,[b] AND JONAS NYCANDER[c]

[a] *Department of Marine Sciences, University of Gothenburg, Gothenburg, Sweden*
[b] *LOCEAN Laboratory, Sorbonne Université-CNRS-IRD-MNHN, Paris, France*
[c] *Department of Meteorology, Stockholm University, Stockholm, Sweden*

(Manuscript received 2 December 2021, in final form 9 March 2022)

ABSTRACT: The stratification is primarily controlled by temperature in subtropical regions (alpha ocean) and by salinity in subpolar regions (beta ocean). Between these two regions lies a transition zone, often characterized by deep mixed layers in winter and responsible for the ventilation of intermediate or deep layers. While of primary interest, no consensus on what controls its position exists yet. Among the potential candidates, we find the wind distribution, air–sea fluxes, or the nonlinear cabbeling effect. Using an ocean general circulation model in an idealized basin configuration, a sensitivity analysis is performed testing different equations of state. More precisely, the thermal expansion coefficient (TEC) temperature dependence is explored, changing the impact of heat fluxes on buoyancy fluxes in a series of experiments. The polar transition zone is found to be located at the position where the sign of the surface buoyancy flux reverses to become positive, in the subpolar region, while wind or cabbeling are likely of secondary importance. This inversion becomes possible because the TEC is reducing at low temperature, enhancing in return the relative impact of freshwater fluxes on the buoyancy forcing at high latitudes. When the TEC is made artificially larger at low temperature, the freshwater flux required to produce a positive buoyancy flux increases and the polar transition moves poleward. These experimets demonstrate the important role of competing heat and freshwater fluxes in setting the position of the transition zone. This competition is primarily influenced by the spatial variations of the TEC linked to meridional variations of the surface temperature.

KEYWORDS: Buoyancy; Intermediate waters; Surface fluxes

1. Introduction

The transition between warm saline subtropical waters and cold fresh subpolar waters is usually very abrupt and has similar structures on the North Atlantic Ocean, the North Pacific Ocean, and the Southern Ocean, suggesting that the same processes lead to these transitions. Not only do the surface temperature and salinity change, but also the way they vary with depth. Subtropical regions are characterized by a decrease of the temperature with depth together with a decrease of salinity: temperature has a stratifying effect while salinity has a destabilizing one. On the contrary, surface temperature is colder than subsurface temperature in polar regions, so temperature destratifies the water column and salinity controls the stable stratification. These two opposite stratification types are referred to as alpha (temperature control) and beta (salinity control) and are representative of middle and high latitudes, respectively, with the beta ocean halocline being essential for the formation of sea ice (Carmack 2007). In between these alpha and beta regions lies a transition zone. Its exact definition varies among authors, but it can often be associated with a surface density maximum (Roden 1970). It contains a weak stratification, making it an ideal place for connecting surface and intermediate water and for increased mixing (Stewart and Haine 2016).

In the Southern Ocean, the transition between alpha and beta ocean is achieved by a succession of fronts closely related to the stratification of the water column and impacting the biological production (Pollard et al. 2002; Pauthenet et al. 2017). These frontal areas are the place of formation of Antarctic Intermediate Water (AAIW) and Subantarctic Mode Water (SAMW). The mixed layer (ML) is deep in winter, and the water escapes the seasonal thermocline to reach the permanent one through lateral subduction (Piola and Georgi 1982; Marsh et al. 2000; Holte et al. 2012; Sallée et al. 2010). A similar ventilation process occurs in the North Atlantic (Woods 1985).

The ventilation of the thermocline in the subtropical gyres is primarily induced by Ekman downwelling (Marshall et al. 1993; Karstensen and Quadfasel 2002). However, in the transition zones of the Southern and North Atlantic oceans, the Ekman vertical velocity is oriented upward, so wind can hardly explain the local downwelling (McCartney 1982; Sallée et al. 2010; Nycander et al. 2015).

The water masses that are exported below the mixed layer must be associated with buoyancy fluxes, whether they come from surface fluxes, diffusive fluxes, advection, or mixing, before taking part of the global overturning circulation (Walin 1982; Speer et al. 2000; Kuhlbrodt et al. 2007; Cessi 2019). The production of AAIW and SAMW results from both horizontal advection induced by wind stress and eddies and from the surface buoyancy fluxes (Sloyan and Rintoul 2001). The surface buoyancy loss during winter produces dense deep

Denotes content that is immediately available upon publication as open access.

Corresponding author: Romain Caneill, romain.caneill@gu.se

DOI: 10.1175/JPO-D-21-0295.1

water in the Nordic seas and surrounding basins (Isachsen et al. 2007; Petit et al. 2020), and their rate of formation is directly impacted by the buoyancy forcing (Mauritzen and Häkkinen 1999). Moreover, buoyancy fluxes and particularly freshwater inputs can damp the creation of deep water in the Labrador seas (Lazier 1980).

The surface heat loss contributes strongly to deepening the mixed layer in the subpolar regions; however, the positive surface freshwater flux present at high latitudes counterbalances the heat loss. Schmitt et al. (1989) studied the relative importance of buoyancy flux due to heat and salt and suggested the idea of a balance between these two effects, but while having high uncertainties due to their flux estimates. The distinction between thermal and haline buoyancy forcing is important for water mass transformation (Speer et al. 1995; Karstensen and Lorbacher 2011). The effect of heat and freshwater fluxes on the buoyancy fluxes needs to be studied carefully as the equation of state (EOS) for seawater is nonlinear.

The buoyancy is a function of the active tracers, temperature, and salinity through the equation of state for seawater. The contribution of temperature and salinity to buoyancy are scaled by the thermal expansion coefficient (TEC) and the haline contraction coefficient (HCC), respectively (Roquet et al. 2015). These coefficients describe how much the density changes when temperature or salinity changes. While the HCC varies by less than 10% in the ocean, the TEC is highly dependent on temperature and pressure. It increases almost linearly with temperature and is about 9 times smaller in polar regions than in the tropics. Variations of the TEC are responsible for the two main nonlinearities in the EOS: cabbeling (variation with temperature) and thermobaricity (variation with pressure). It is known that these nonlinearities have a nonnegligible impact on water mass transformations, as they can cause diapycnal advection from isopycnal diffusion (e.g., Garrett and Horne 1978; McDougall and You 1990; Iudicone et al. 2008; Klocker and McDougall 2010; Stewart and Haine 2016; Thomas and Shakespeare 2015). The overall result of cabbeling is that at steady state, when the time- and spaced-averaged surface heat and freshwater fluxes vanish, the average surface buoyancy flux is positive, compensating the interior buoyancy sink due to cabbeling (Hieronymus and Nycander 2013).

Another implication of the TEC variation is that the buoyancy loss associated with a heat loss depends on the value of the TEC, itself a strong function of temperature. As the surface buoyancy flux in subpolar regions results from a competition between its thermal and haline components, it is likely that the decrease of the TEC at low temperature increases the relative haline influence, as pointed out by Rooth (1982), Bryan (1986), and Aagaard and Carmack (1989). The nonlinearities are found to be important in the global circulation and to contribute to setting the global ocean properties. A difference of mean salinity and temperature along with differences of circulation are found when using a linear EOS on a realistic ocean global circulation model compared to a realistic EOS (Roquet et al. 2015; Nycander et al. 2015). However, the buoyancy fluxes have not been accurately studied in the cited studies.

This study aims to investigate how the location of the polar transition (between alpha and beta ocean) and of the intermediate water location are influenced by the surface buoyancy flux, and especially by its latitudinal change of sign. As the buoyancy flux is strongly linked to the TEC in the polar area, modifying the parameters for the EOS in a numerical model study is used here as an effective method to modulate the relative impact of heat and freshwater on the surface buoyancy flux. The stratification is also impacted, while keeping similar surface temperature and salinity fields and the same wind forcing between the experiments. For the numerical experiments, an idealized configuration of the NEMO (Nucleus for European Modeling of the Ocean; Madec et al. 2019) ocean general circulation model (OGCM) has then been developed, using a simplified EOS allowing for a full control of its nonlinearities (Roquet et al. 2015).

This paper is organized as follow. The equation of state for seawater, its properties, and the stratification control index are presented in section 2. The model configurations are then described in section 3, followed by the description and analysis of the reference run (section 4). A comparison of the different parameter is then discussed (section 5) and further discussions and conclusions are given in section 6.

2. The equation of state for seawater

a. General properties

The EOS for seawater gives the density as a function of temperature, salinity, and pressure. Under the Boussinesq approximation, the thermal expansion coefficient α and the haline contraction coefficient β are defined as

$$\alpha = -\frac{1}{\rho_0}\left.\frac{\partial \rho}{\partial \Theta}\right|_{S_A,p}, \tag{1}$$

$$\beta = \frac{1}{\rho_0}\left.\frac{\partial \rho}{\partial S_A}\right|_{\Theta,p}. \tag{2}$$

We use here the Conservative Temperature Θ and Absolute Salinity S_A following the TEOS-10 standard (McDougall 2003; IOC et al. 2015), but for simplicity we will call them temperature and salinity in the rest of the paper.

The surface buoyancy fluxes are related to the fluxes of heat and freshwater, weighted by the TEC and HCC, and can be decomposed into their respective contributions:

$$F_b = \underbrace{\frac{g\alpha}{\rho_0 C_p} Q_{\text{tot}}}_{F_b^\Theta} + \underbrace{\frac{-g\beta}{\rho_0} f_S}_{F_b^S}, \tag{3}$$

where g is the gravity acceleration, $C_p \simeq 3991.86$ J kg^{-1} K^{-1} the heat capacity, Q the total heat flux (W m^{-2}), and $f_S = S_{\text{surf}}(E - P)$ the equivalent salt flux in (g kg^{-1}) kg m^{-2} s^{-1}, linked to the evaporation E and precipitation P (both in kg m^{-2} s^{-1}), through the surface salinity S_{surf}. The term F_b^Θ is the heat contribution, F_b^S the salt contribution, and F_b the total surface buoyancy flux (m^2 s^{-3}). We define the buoyancy flux using a

TABLE 1. Default value of the simplified equation of state coefficients.

Coefficient	Value	Description
a_0	1.65×10^{-1} °C^{-1} kg m^{-3}	Linear thermal expansion coefficient
b_0	7.6554×10^{-1} (g kg^{-1})$^{-1}$ kg m^{-3}	Linear haline expansion coefficient
C_b	9.9×10^{-3} °C^{-2} kg m^{-3}	Cabbeling coefficient
T_h	2.4775×10^{-5} °C^{-1} dbar^{-1} kg^{-3}	Thermobaric coefficient

salt flux and not a freshwater flux as salinity restoring conditions creating a salt flux are used in the model configuration.

b. The simplified equation of state

Roquet et al. (2015) proposed a simplified version of the EOS that retains the main nonlinearity of the EOS while being analytically tractable, so that the TEC is linearly dependent on the temperature and the pressure and the HCC is constant. This simplified version of the nonlinear EOS produces realistic ocean properties when applied on OGCMs, in contrast to a linear EOS where both the TEC and HCC are constant (Nycander et al. 2015). Were we use this simplified equation of state, i.e.,

$$\rho(\Theta, S_A, p) = \rho_0 - \left(a_0 + \frac{1}{2} C_b \Theta_a + T_h p\right)\Theta_a + b_0 S_a, \quad (4)$$

with $\Theta_a = \Theta - 10$°C, $S_a = S_A - 35$ g kg^{-1}, and p the pressure. Table 1 gives the standard values and description of the coefficients of the EOS. The T_h term sets the thermobaricity dependence and is kept for realistic representation of the deep circulation, but is kept constant in all the experiments. The dependence of the TEC on the temperature and the constant value of the HCC are evident using this simplified EOS, as they become

$$\alpha = \frac{1}{\rho_0}(a_0 + C_b \Theta_a + T_h p), \quad (5)$$

$$\beta = \frac{b_0}{\rho_0}. \quad (6)$$

This simplified equation is used to compute the density and buoyancy flux in the different runs of the circulation model used in this study.

c. The stratification control index

Changes in Θ or S_A lead to changes of the density that affect the circulation and stratification. The stratification control index (SCI) is defined such as to compare the relative effect of temperature and salinity on the stratification:

$$\mathrm{SCI} = \frac{N_\Theta^2 - N_S^2}{N_\Theta^2 + N_S^2}, \quad (7)$$

$$N^2 = -\frac{g}{\rho_0}\frac{\partial \rho_\Theta}{\partial z} = N_\Theta^2 + N_S^2, \quad (8)$$

TABLE 2. The different parameters of the simplified EOS for the five runs. The other parameters are kept constant and equal to the default values.

Name	a_0 (°C^{-1} kg m^{-3})	C_b (°C^{-2} kg m^{-3})
Ref	1.65×10^{-1}	9.9×10^{-3}
A	1.65×10^{-1}	13.2×10^{-3}
B	1.45×10^{-1}	8.7×10^{-3}
C	1.85×10^{-1}	11.1×10^{-3}
D	1.65×10^{-1}	6.6×10^{-3}

$$N_\Theta^2 = g\alpha \frac{\partial \Theta}{\partial z}, \quad (9)$$

$$N_S^2 = -g\beta \frac{\partial S_A}{\partial z}. \quad (10)$$

Two critical transitions occur, when SCI = 1 (no salinity stratification) and SCI = −1 (no temperature stratification). This means that three states of the stratification can be expected:

1) SCI $\geq$ 1, an *alpha ocean* stratified by temperature and destratified by salinity,
2) SCI ≤ -1, a *beta ocean* stratified by salinity and destratified by temperature,
3) $-1 <$ SCI < 1, a *transition zone* doubly stratified by both temperature and salinity.

Note that the SCI has not been defined previously in the literature to our knowledge. However, it can be directly linked to standard indexes, such as the Turner angle [SCI = tan(Tu)] or the density ratio, $R_\rho = -N_\Theta^2/N_S^2$ (Ruddick 1983). For stable stratifications ($N^2 > 0$), the SCI is uniquely defined over the real numbers and has the advantage to treat symmetrically the effect of salinity and temperature and avoid singularities, contrary to the density ratio. We therefore chose to focus on this new index here.

The SCI will be computed 10 m below the mixed layer, from monthly mean values. For every longitude–latitude point the SCI at the time of deepest mixed layer will be retained for the ocean classification. Thus, we classify the ocean based on the permanent thermocline, and not on the seasonal one. Note that our definition of the alpha, beta and transition zones differ slightly from previous ones (Carmack 2007; Stewart and Haine 2016). We retain our definition to get a unique decomposition between the three ocean types.

3. The model configurations

In a series of sensitivity experiments, the parameters that control the surface TEC dependance on temperature, a_0 and C_b, are modified between each run. A total of five different parameter combinations are used (Table 2).

a. Description of the model

The NEMO (Madec et al. 2019) OGCM is used for the simulation. The configuration represents an idealized basin on the sphere, 40° of longitude wide, and from 0° to about 60°N,

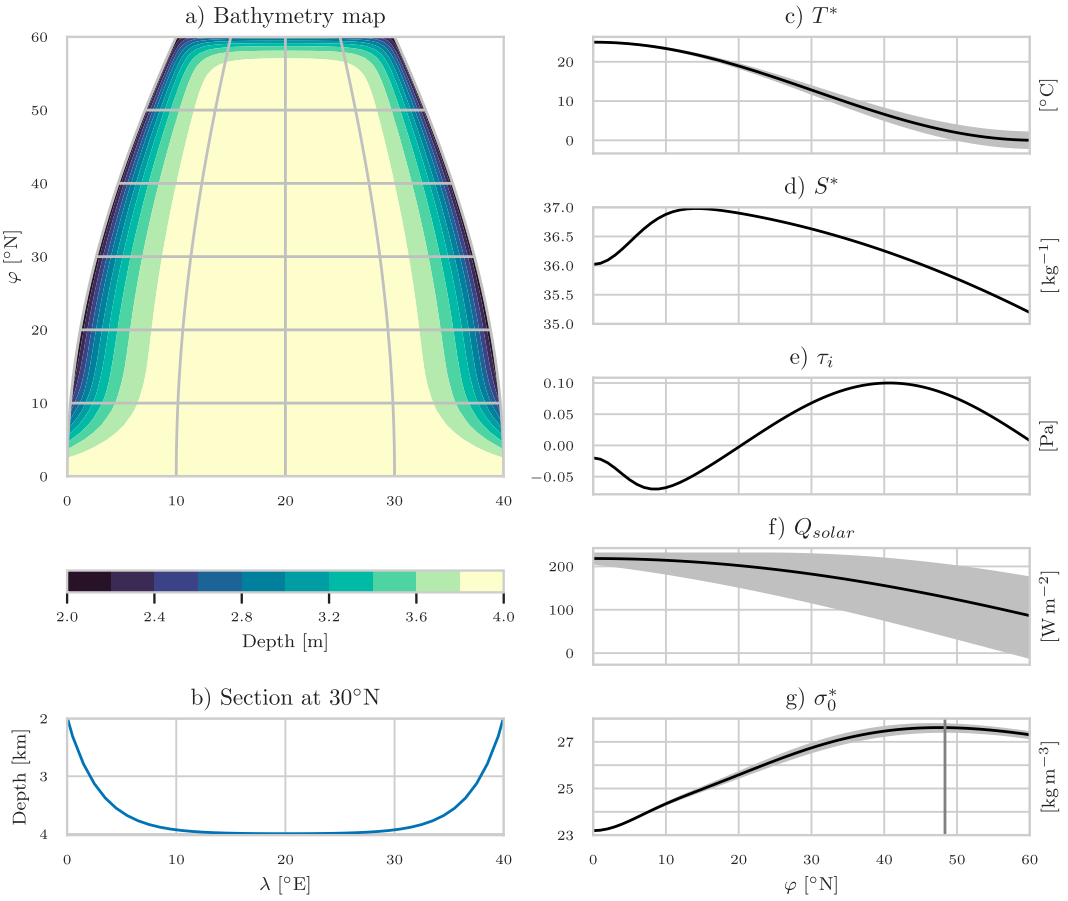

FIG. 1. (a),(b) Bathymetry of the basin. Forcing fields used by the model, with (c) the restoring temperature, (d) the restoring salinity, (e) the zonal wind stress, (f) the solar heat flux, and (g) the restoring density anomaly. The average values are plotted in black. For (c), (f), and (g), the gray zone represents the seasonal variation range. The vertical line in (e) represents φ_M, the latitude of the winter maximum restoring density.

similar to the one of Lazar et al. (1999). The width of the basin (in meters) decreases with latitude, and the Coriolis parameter is computed as $f = 2\Omega \sin(\varphi)$. A 1° longitude Mercator grid is used so the resolution (in meters) scales as cos(latitude), the number of grid points is 42 in longitude and 79 in latitude. The topography in meters is represented by an exponential slope with a length scale of 3°:

$$h(\lambda) = 4000 - 2000\left[\exp\left(-\frac{\lambda}{3}\right) + \exp\left(\frac{\lambda - 40}{3}\right)\right], \qquad (11)$$

with λ the longitude. A similar topography applies at the northern boundary, using the latitude coordinate. The bathymetry along the coast is 2000 m and reaches 4000 m in the central basin (Figs. 1a,b). A nonlinear free surface is used. The time step is 45 min. A terrain following coordinate is used, where the five upper levels have a constant thickness of 10 m, and the thickness then increases to 440 m at the bottom of the deepest parts, for a total of 36 vertical levels. To minimize the ageostrophic current due to the error on the pressure gradient caused by the terrain following coordinates close to the equator, the topography is flattened around the equator at the depth of 4000 m. Symmetric boundary conditions are used at the equator, with a no meridional fluxes condition applied. This symmetrical condition is equivalent to having a two hemispheres model forced with the same forcing, and only retain the Northern Hemisphere, while only computing the northern one.

The effect of unresolved eddies is parameterized using the Gent and McWilliams (1990) formulation, and lateral mixing is done along the neutral plane. A turbulent kinetic energy (TKE) closure is used to compute the vertical viscosity and diffusivity coefficients, with background values set to 10^{-4} m^2 s^{-1}. This high vertical diffusivity value allows a high consumption of bottom water through vertical turbulent diffusion and thus a sufficiently strong overturning circulation.

b. *Forcing fields*

The model is forced by analytical fields that represent the zonal wind stress, the heat, and haline fluxes. The analytical functions have been inspired and adapted from Lévy et al. (2010) and Wolfe and Cessi (2014), chosen to represent zonal

averages over the ocean. The thermal and haline forcing are both represented by a relaxation law so the surface fluxes are proportional to the difference between a restoring value and the ocean surface value:

$$Q_{\text{tot}} = A_\Theta(T^* - \text{SST}), \tag{12}$$

$$f_S = A_S(S^* - \text{SSS}), \tag{13}$$

with $A_S = 3.858 \times 10^{-3}$ kg m^{-2} s^{-1} the haline restoring coefficient, $A_\Theta = 40$ W m^{-2} °C^{-1} the temperature restoring coefficient, and SST (SSS) the sea surface temperature (salinity). The restoring fields are defined by the following equations:

$$T^* = [T_{\text{eq}} - T_N(d)]\cos^2\left(\frac{\pi\varphi}{2L}\right) + T_N(d), \tag{14}$$

$$T_N(d) = \Delta T \cos\left(\pi\frac{d + 159}{180}\right), \tag{15}$$

$$S^* = S_0 \exp\left[-\left(\frac{\varphi}{260}\right)^2\right] - S_1 \exp\left[-\left(\frac{\varphi}{7.5}\right)^2\right], \tag{16}$$

where $T_N(d)$ represents the seasonal variation of T^* with the respect of the day of the year d and φ the latitude in degrees. $T_{\text{eq}} = 25$°C is the temperature at the equator, $\Delta T = 2$°C, $L = 61$°C is the approximate latitudinal basin extension, $S_0 = 37.12$ g kg^{-1}, and $S_1 = 1.1$ g kg^{-1}.

The heat flux is split into a shortwave (solar) part and the nonsolar remainder:

$$Q_{\text{solar}}(\varphi, d) = 230\cos\left[\pi\frac{\varphi - 23.5\cos\left(\pi\frac{d + 189}{180}\right)}{0.9 \times 180}\right], \tag{17}$$

$$Q_{\text{non solar}} = Q_{\text{tot}} - Q_{\text{solar}}. \tag{18}$$

The solar part is applied with a day/night cycle and is split into two bands with e-folding depths of 23 m (fraction 42%) and 0.35 m (fraction 58%) (Madec et al. 2019). The seasonal variation of the heat forcing induces a thermal restratification in summer, while the penetrative heat flux helps to reduce the upper stratification and limits the minimum mixed layer depth in tropical regions. We emphasize, however, that the results of our study are not sensitive to these details.

From the restoring fields, it is possible to define a restoring density anomaly σ_0^*, defined as the density anomaly of water at the surface, with a temperature T^* and a salinity S^*, along with the latitude φ_M where this forcing density is maximum:

$$\sigma_0^* = \rho(T^*, S^*, 0) - 1000 \quad \text{and} \quad \sigma_0^*(\varphi_M) = \max(\sigma_0^*). \tag{19}$$

For the reference run, this latitude is equal to 48.3°N.

The zonal wind stress follows the equation

$$\tau_\lambda = 0.1\left[-\cos\left(\frac{3\pi\varphi}{2L}\right) + 0.8\exp\left(-\frac{\varphi^2}{5.77^2}\right)\right]. \tag{20}$$

These fields are plotted in Fig. 1. The restoring temperature decreases from 25°C at the equator to 0°C on average at 60°N (−2°C in winter and 2°C in summer). The winter also corresponds to the period with less solar flux, which encounters a higher seasonality at high latitude than at the equator.

Several critical processes are missing here to obtain a realistic forcing, including the absence of interactive atmosphere and of sea ice, as the restoring temperature is too high to allow the formation of sea ice. We return to the potential limitations of not including sea ice formation in our configuration in section 6.

The model is run 2000 years for each simulation until equilibrium with level averages of temperature and salinity trends below 0.1°C and 0.01 g kg^{-1} per millennium, respectively. Fifty-year mean fields are used for all the subsequent analyzes, except for the SCI and for the mixed layer depth, where monthly averages are used.

4. Reference run

a. General description

The reference run uses the reference parameters for the EOS defined in Table 1 and is labeled as ref. The wind stress is kept constant between the different runs. As the barotropic streamfunction depends to first order on the wind stress, it is very similar for all the runs. It is shown in Fig. 2 along with the theoretical Ekman vertical velocities at the bottom of the Ekman column. The three expected gyres are present: an equatorial gyre from 0° to 10°N, a subtropical gyre from 10° to ~40°N, and a subpolar gyre from ~40° to 60°N. The theoretical Ekman vertical velocity w_{Ek} shows downwelling south of 34.8°N and upwelling north of this latitude. The w_{Ek} is computed using the following formula in spherical coordinates (Pedlosky 1996, chapter 1):

$$w_{\text{Ek}} = -\frac{1}{\rho_0}\frac{1}{R\cos\varphi}\frac{\partial}{\partial\varphi}\left(\frac{\tau_\lambda\cos\varphi}{\rho_0 f}\right), \tag{21}$$

where R is Earth's radius.

Figure 3 shows the overturning streamfunctions in density coordinates. The reference depth used for the potential density does not have a major impact on the results, thus σ_0 referenced at the surface is used. The surface circulation induced by the wind is visible at low latitude. A deeper cell corresponds to the deep circulation induced by the surface buoyancy forcing. This circulation is weak but oriented toward the equator.

Figure 4 shows the mean SST, SSS, and surface density anomaly (σ_0) of the reference run. The main features expected to be produced by the model are present: a strong western boundary current visible in the SST and the SSS, advecting warm and salty water between about 10° and 45°N, an equatorial upwelling at the eastern side, high salinity forced by net evaporation in the subtropics and low salinity (precipitation zones) close to the equator and in the subpolar region, while a cold freshwater pool is found on the northwest part of the basin.

The lowest densities are found in the western tropics, where the warmest SST are found. By contrast, the densest surface waters are not found at the coldest SST, due to the compensating

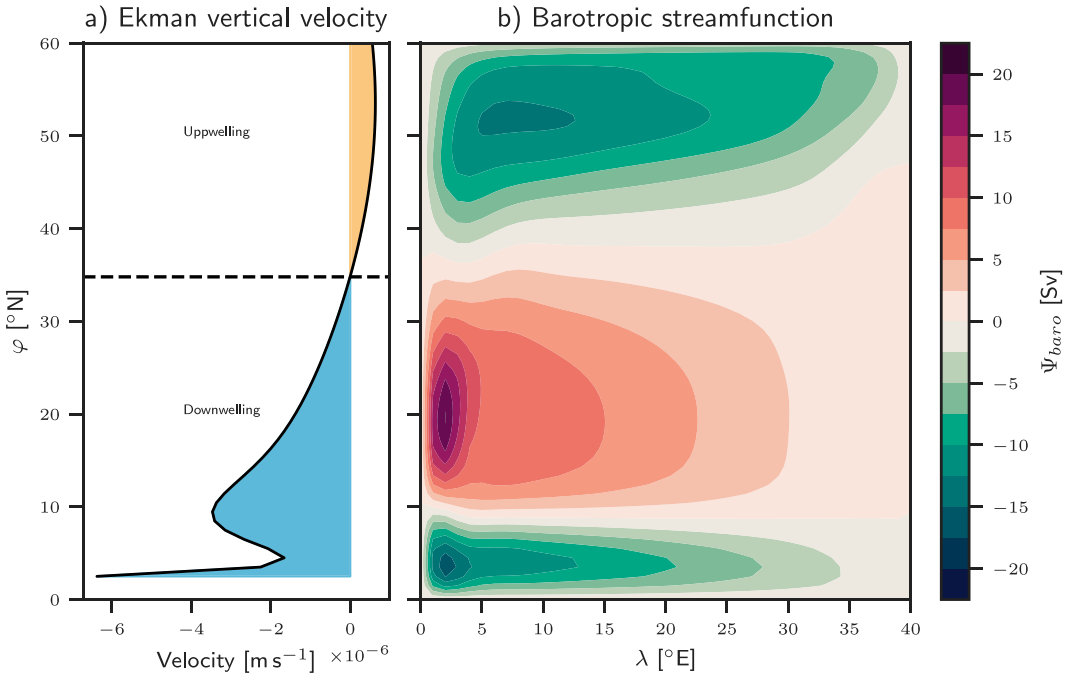

FIG. 2. Wind induced circulation: (a) theoretical Ekman vertical velocity and (b) barotropic response for the reference run. The Ekman velocity is not shown south of 2°N, as it diverges to $-\infty$.

effect of salt. They are located in the northeast area of the basin, while the coldest water is in the northwest, in a very fresh area. The maximum surface density anomaly is smaller than the maximum of σ_0^*. However, in similar runs without seasonality in the forcing fields, the surface maximum density anomaly is larger than the maximum of σ_0^*, due to advection of salty water in a cold region (figure not shown).

The western boundary current is visible on the sea surface height (SSH; Fig. 5a). An eastern boundary current is also visible in the eastern side, north of 30°N. These two currents advect warm and salty water in direction of the pole, and under the restoring condition these water masses will lose both heat and salinity.

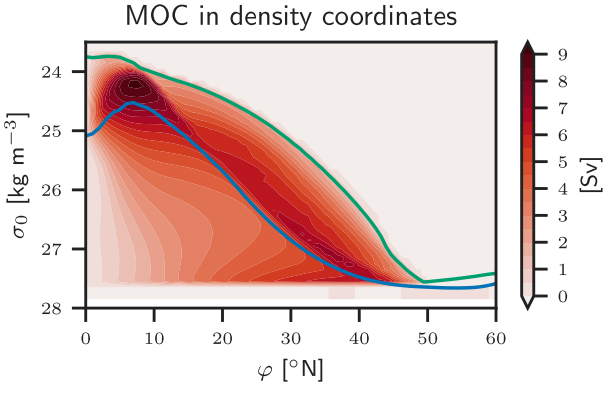

FIG. 3. Meridional overturning streamfunction computed in density coordinates. The green and blue lines represent the zonal minimum and maximum surface densities, respectively. Following standard conventions, the circulation is clockwise around maximum streamfunction values.

The annual maximum of the mixed layer depth (MLD) is shown in Fig. 5b. We use a density criterion with a threshold of 0.01 kg m^{-3} (de Boyer Montégut 2004). Because of the seasonality of the heat forcing, the mixed layer gets shallower in summer and deepens in winter, especially in the northern part of the basin where the temperature seasonality is the most important. Looking at the annual maximum reveals the deep convective area, which is situated in the northeast part of the basin. The fresh and cold pool visible on the SST and SSS maps appears to be very stratified and to have a shallow MLD of less than 200 m, compared to more than 3000 m on the eastern side at the same latitude. The SCI at the bottom of the winter ML (Fig. 5c), defined by Eq. (7), shows a sharp demarcation between the alpha (in red) and beta ocean (in blue) around 50°N. The northwest fresh pool is a beta ocean, implying that the salinity increases with depth (stabilizing effect), but that the temperature also increases (destabilizing effect). This means that deep water is saltier and warmer than the water in the mixed layer, implying that this deep water has been formed in a warmer area. A very narrow transition zone (surrounded by the white contour in the figure) lies between the alpha and beta ocean.

The alpha–beta front matches closely the northern limit of the deep ML region. Indeed, the beta region arises from the fact that fresh and cold water lies over saltier and warmer water. This deeper water comes from the deep ML region where it convects and is then advected into the northwest pool.

Figure 6 presents two sections of the SCI, at the end of the winter, when the mixed layer is the deepest, and at the end of

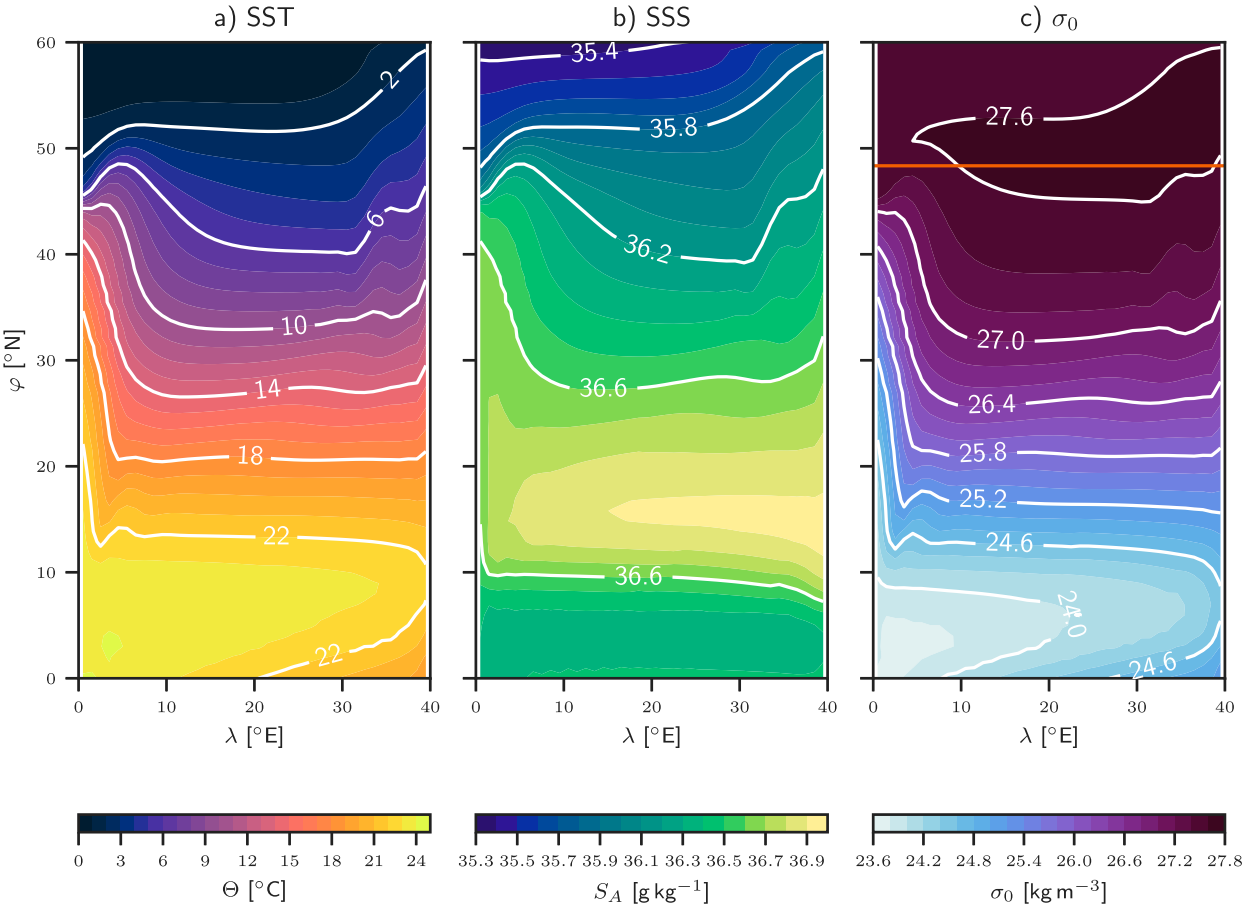

FIG. 4. (a) SST, (b) SSS, and (c) surface density anomaly for reference run. The horizontal orange line in (c) indicates φ_M.

the summer when the surface layers are the most stratified. The shallow fresh pool is visible north of 50°N, where the ocean is stratified by the salinity in the upper 100 m, particularly in the section 1 (at λ = 14.5°E). Apart from this small area, the majority of the ocean is classified as alpha ocean and a transition zone area exists between 40° and 50°N, close to the surface, and in the tropical region, and below 2000 m alpha ocean prevails. Due to the annual cycle of the thermal forcing, restratifying thermally the ocean in summer, the beta region is limited in its depth. On both sections it is seen that this shallow layer of beta ocean acts as a lid that prevents convection in winter. A control run conducted without the annual cycle shows deeper beta region in the north (not shown).

b. *Buoyancy forcing and response*

Following Eq. (3), Fig. 7 presents the surface buoyancy flux and its decomposition into the thermal and haline components. The annual-mean surface buoyancy flux sets the surface density change induced by the external forcing; we thus use the yearly averages of the surface buoyancy flux. The southern part of the basin gains heat while the northern part loses it. The fluxes are small around 10°N, where the surface velocity is zonal and the mixed layer shallow, leaving enough time for the water to thermally equilibriate with the forcing. The most negative buoyancy fluxes due to heat are found in the vicinity of the western boundary current, where warm water is advected northward.

The maximum values of F_b^Θ are roughly 10 times larger than the maximum values of F_b^S. However, as F_b^Θ is small in the northern part of the basin, these two components are comparable there. Around 55°N, the buoyancy forcing changes sign and becomes positive northward due to the freshening flux. This inversion of the surface flux is possible because 1) the heat flux becomes small in the north and 2) the TEC decreases at low temperature. The effect of this second point is that the influence of the heat flux on the buoyancy flux decreases in the polar regions. The densest surface water must be located in an area of buoyancy loss, so the surface buoyancy flux inversion marks a northern limit for the surface densest water. Moreover, this densest surface water is located where the mixed layer is deepest, i.e., in the convective zone.

5. Comparison with different parameters in the EOS

In the reference run the position where the surface buoyancy flux changes sign in the north is well correlated with the position of the alpha–beta front. This front also corresponds to the northern boundary of the deep ML area and the southern

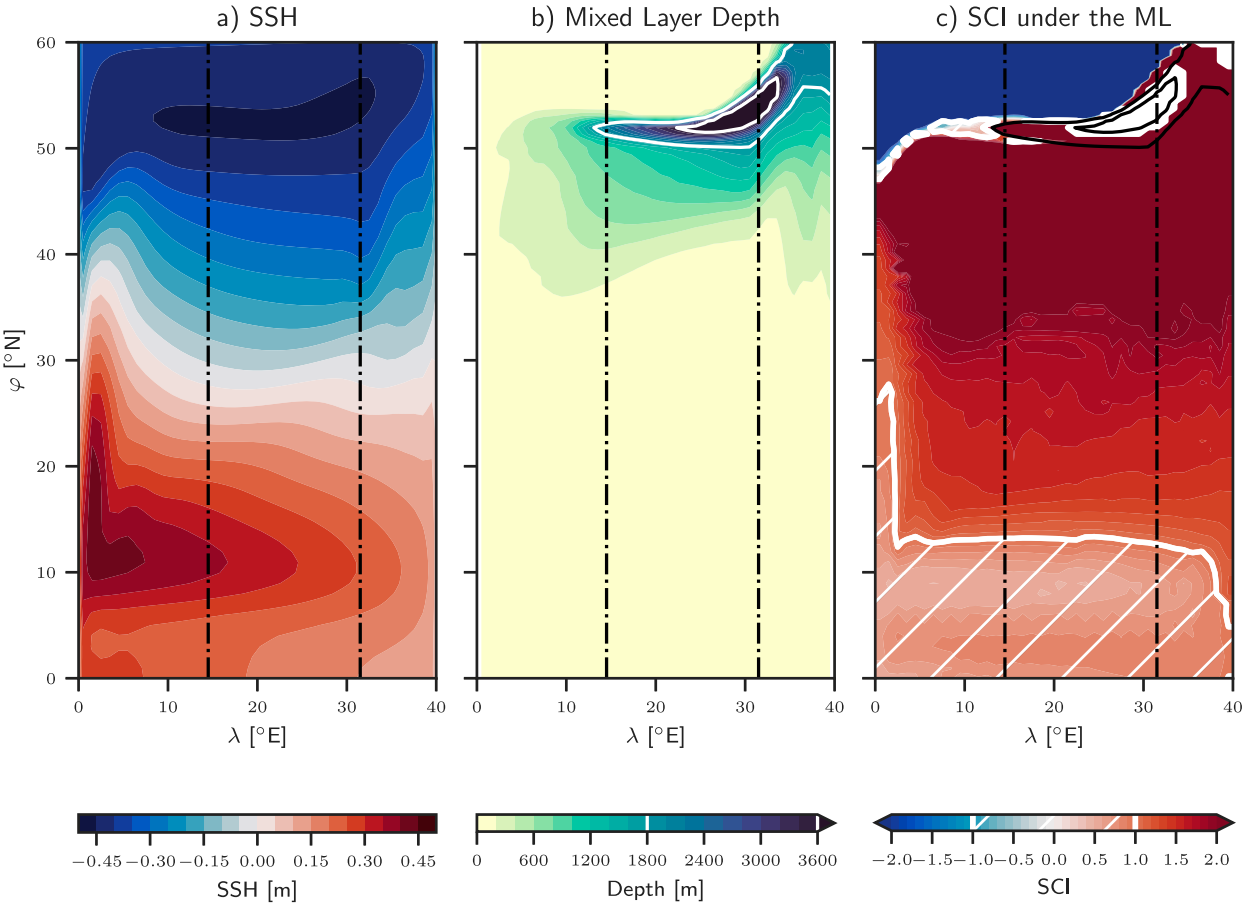

FIG. 5. (a) Sea surface height, (b) annual deepest mixed layer depth, and (c) stratification control index under the mixed layer for the reference run, taken in each point at the time of the year when the mixed layer is the deepest. The white contour in (c) indicates the transition zone, i.e., $-1 < \mathrm{SCI} < 1$, while the two black contours emphasize the 1800- and 3600-m MLD [these contours correspond to the two white contours of (b)]. When the mixed layer reaches the bottom cell, no value is used for the SCI (white areas). The black dashed lines represent the location of the sections presented in Fig. 6.

boundary of the northwest fresh pool. This section studies the causality hidden behind this correlation. Added to the reference experiment, four sensitivity runs have been conducted, with changes of the EOS parameters (Fig. 8a), resulting in different variations of the TEC with temperature. The wind is kept unchanged between the different runs.

Figure 9 shows the total surface buoyancy flux for the five experiments, along with the position of the beta boundary (SCI = −1) (the white line with a black contour). The runs are ordered with increasing polar TEC value from left to right (Fig. 8b). In this way, the experiments are organized with a relative decrease (increase) of the salinity (temperature) effect from left to right. Even if not exactly located at the same place, the positions of the polar transition zone and the buoyancy flux inversion are very close and follow a similar evolution between the runs. For higher values of the TEC (lower relative salinity impact) the transition zone is pushed to the north of the basin, where the salt fluxes eventually take control of the buoyancy flux. On the contrary, if the TEC is small, the heat flux will have a smaller impact on the buoyancy flux (as it is scaled by it) and the salinity control arises more to the south. The more the alpha–beta boundary is pushed to the north, the more it becomes affected by the subpolar gyre, and loses its zonality to become more meridional. The beta ocean is associated with shallow MLD, and a deep ML is found just south of the beta boundary (Fig. A1, appendix A).

The locations of the polar transition zone and of the buoyancy flux inversion are not perfectly zonal due to the effect of the subpolar gyre. However, it is possible to compute an equivalent average latitude, which corresponds to the southern latitude of a zonally uniform ocean, sharing the same integrated area that the area of interest (either the area SCI < −1 or of buoyancy gain in the subpolar region). The detail of the calculation is given in appendix B. The φ_b is the equivalent latitude of the buoyancy flux inversion and φ_β the southern latitude of the fresh beta area. We use φ_β as a proxy for the latitude of the polar transition, as its latitudinal extension is very narrow in our experiments.

These two latitudes increase when φ_M increases, emphasizing the role of the buoyancy forcing (Fig. 10a). When buoyancy

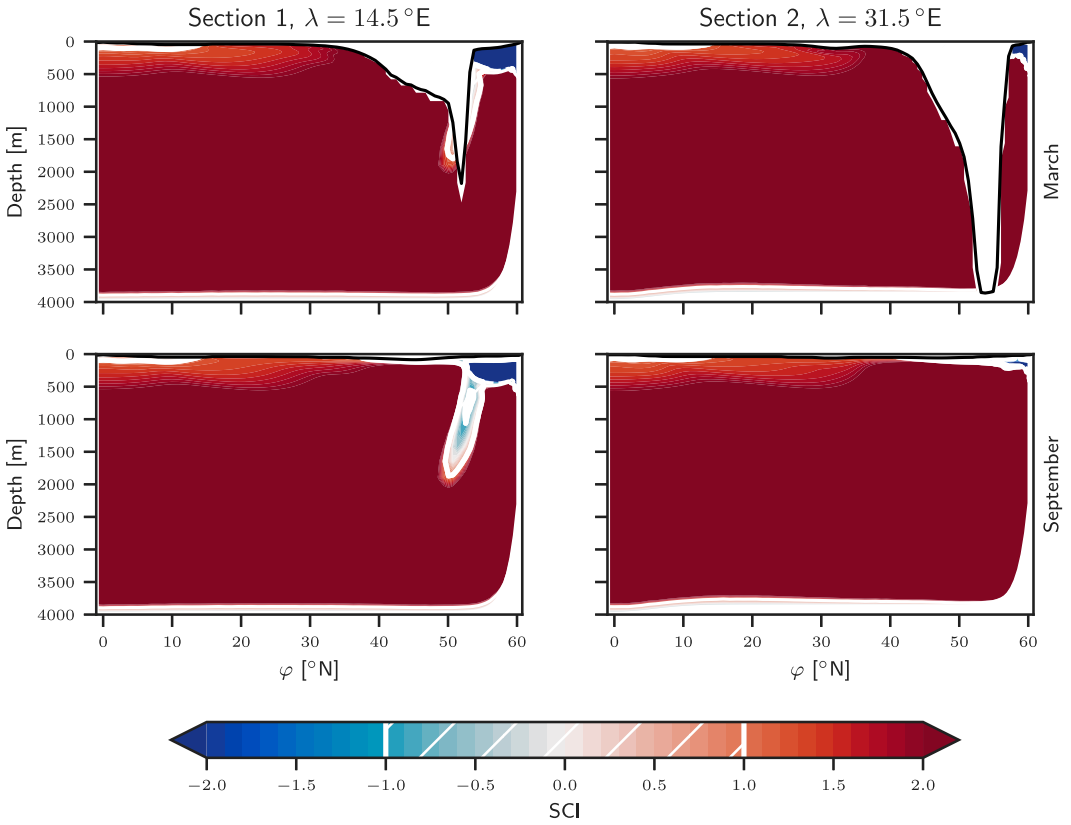

FIG. 6. Sections of the SCI in March and September for the longitudes 14.5° and 31.5°E. The mixed layer reaches the bottom in March at 31.5°E, and below 2000 m all the ocean has a SCI greater than 2.

flux inversion latitude increases, this pushes the beta ocean further north, as shown in Fig. 10b. As the wind is unchanged between the five experiments, the effect of the Ekman pumping cannot be the direct driving effect of the change of latitude of the transition zone. In contrast, the buoyancy forcing is modified at leading order. More specifically, as heat and salt play opposite roles for the buoyancy flux in the northern region, the location where they exactly balance and where the buoyancy flux has an inversion is not only function of their amplitude but also function of the variable TEC. So if the TEC value in the polar region increases, the latitude of the buoyancy inversion increases as well (Fig. 10c). In contrast, the latitude of both buoyancy inversion and polar transition are not monotonically varying with C_b (Fig. 10d).

Changing the TEC and the position of the deep-water creation also changes the properties of the abyssal water (Figs. 10e,f). When the buoyancy inversion is moved northward, the bottom water becomes consequently colder and fresher. As a result, the basin average of both salinity and temperature decrease, with a value of about 0.2 g kg^{-1} and 2°C, respectively, for the range of the experiments.

6. Discussions and conclusions

We have studied here the control of the position of the polar transition zone by the air–sea buoyancy fluxes, particularly by the competition between opposing heat and freshwater surface fluxes. We used an idealized configuration of the OGCM NEMO to verify the hypothesis that the wind or the cabbeling effect are not the main driver of the alpha–beta transition, and that they are not setting the position of the convergence zone and subduction, but on the contrary that the buoyancy fluxes are leading the control. As the relative effect of the heat and freshwater fluxes on the buoyancy fluxes is scaled by the TEC, we modified the equation of state for seawater while restoring the surface temperature and salinity toward the same fields to change the magnitude of these fluxes. When the value of the TEC was artificially increased in the subpolar region, the effect of temperature on stratification and buoyancy flux was made stronger, decreasing the relative impact of salinity fluxes.

The reference run uses a simplified nonlinear EOS with parameters that best fit the TEOS-10 standard (Roquet et al. 2015). The resulting circulation is close to the expected one for a closed basin with three gyres. A striking point is that the convective zone is located immediately south of the beta region. It is easily understood why deep convection cannot occur in the beta region. Since the stratification near the surface is there controlled by the salinity, the winter cooling cannot destabilize the water column. In other words, the capping layer of freshwater prevents convection in the beta region.

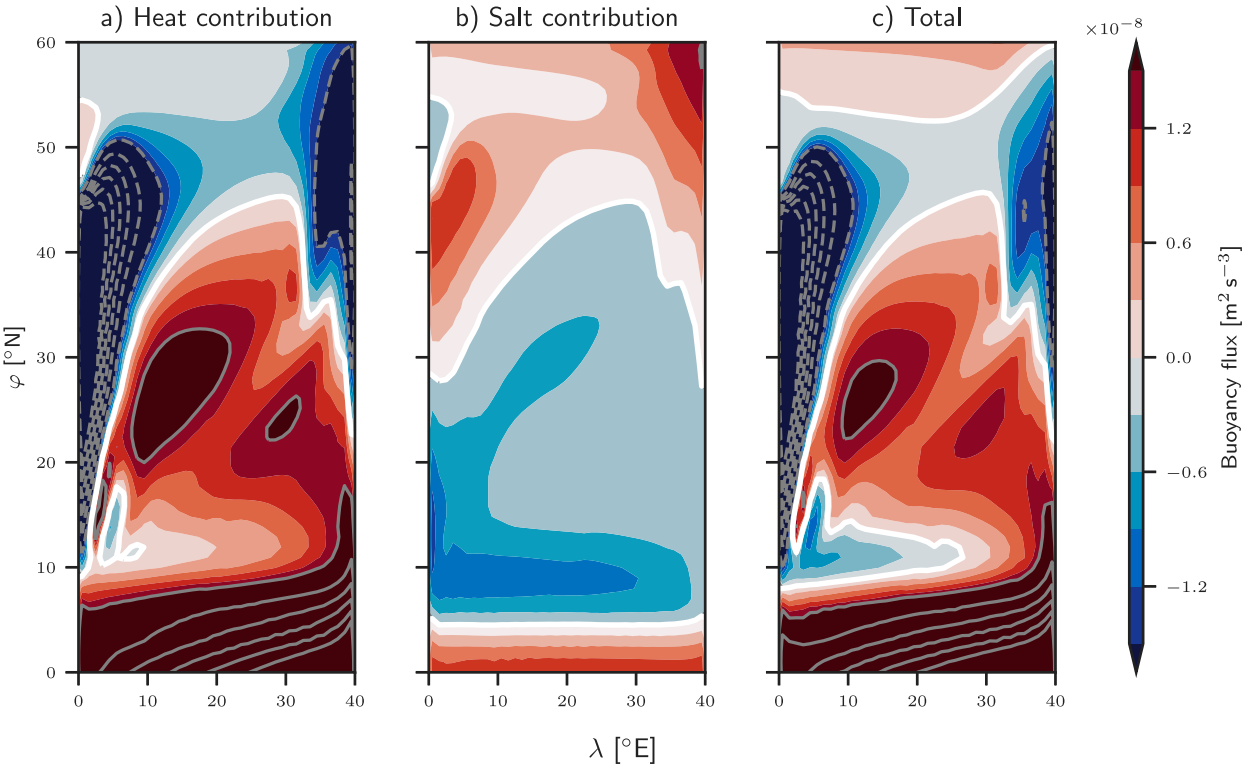

FIG. 7. Buoyancy fluxes: (a) the heat contribution, (b) the salt contribution, and (c) the total flux. The colors are saturated at $\pm 1.5 \times 10^{-8}$ m^2 s^{-3} so that the variations of the salt contribution are visible. The gray lines are separated by 1.5×10^{-8} m^2 s^{-3}, and the white line here underlines the 0 m^2 s^{-3} contour.

The maximum surface densities occur in the convective zone. It has been noted in the past that the transition zones in the Northern Hemisphere are indeed located in areas of local maximum density and low stratification (Roden 1970; Stewart and Haine 2016). If the surface water is denser than the water below the mixed layer, the column becomes unstable and the mixed layer deepens. This dense water may escape the seasonal thermocline and ventilate the permanent thermocline through lateral advection, a process reminiscent of the formation of North Atlantic Deep Water in the North Atlantic basin. Due to the large seasonality of the thermal forcing, the convective region is likely to become stratified by temperature in summer. The densification of surface water happens where surface buoyancy fluxes are negative. If dense water is advected into a region of positive surface buoyancy fluxes, it becomes lighter and thus contributes to making the mixed

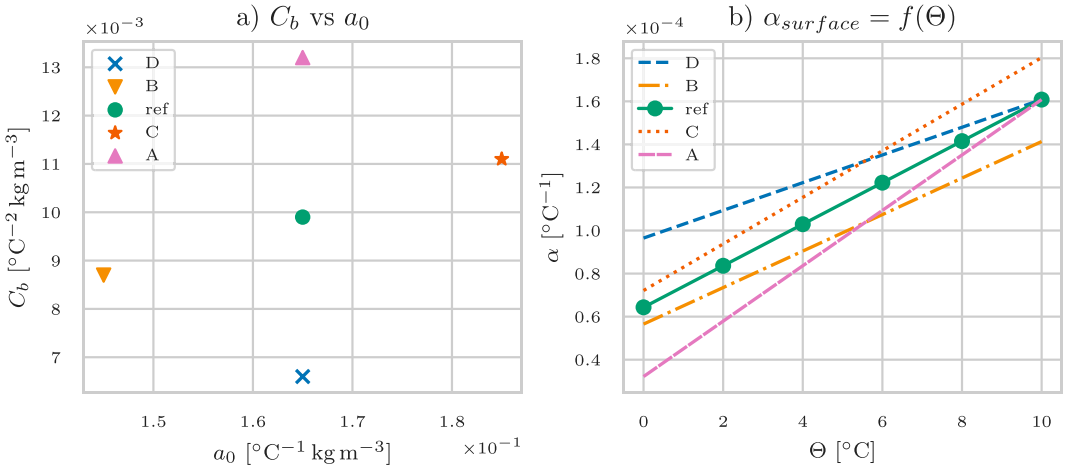

FIG. 8. (a) C_b vs a_0 scatterplot, and (b) variation of the TEC with respect of the temperature for the five experiments.

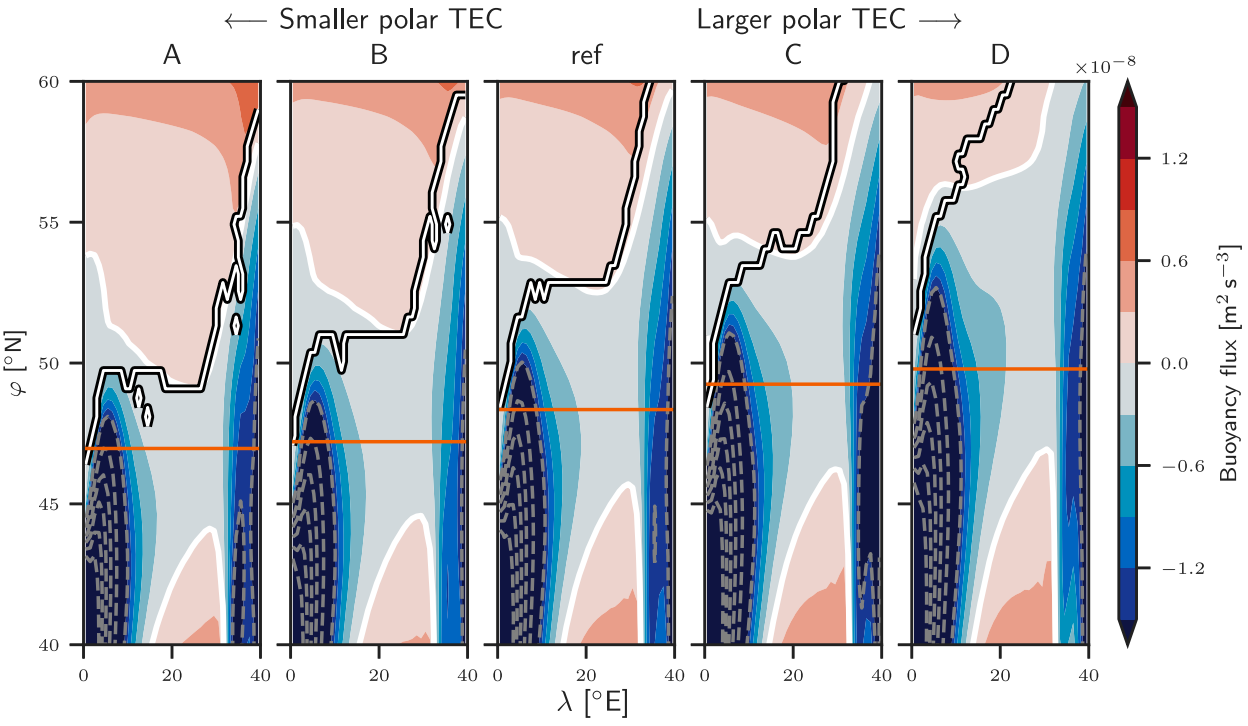

FIG. 9. Net buoyancy flux for every run. No major difference is visible south of 40°N so the figures have been cropped. The white line with black contour represents the −1 value of the SCI under the ML. As the polar transition zone is very narrow between the alpha and beta oceans, this line corresponds very well to the transition between the alpha and beta oceans. The orange line represents the latitude of φ_M, the latitude of maximum value of σ_0^*.

layer shallower. This simple mechanism highlights the importance of the position where the sign of the surface buoyancy flux changes, which itself results from a competition between heat and freshwater fluxes.

Figure 11 presents a conceptual view of the buoyancy flux control on the stratification, and on the intermediate water formation. Three regions result from the competition between F_b^Θ and F_b^S: a region a buoyancy loss surrounded by two regions of buoyancy gain. At the surface, water is advected poleward in the region of buoyancy loss (in the eastern part of the basin). This loss leads to an increase of the mixed layer depth, until the surface layer reaches the subpolar region, where the buoyancy fluxes become positive again. A fresh layer stratified by salinity is formed that prevents convection in this region. At depth, the water formed in the deep mixed layer area leaves the winter mixed layer by lateral induction to form the intermediate (or deep) water. This induction is directed equatorward on average, although it is associated with a cyclonic flow in the north before reaching the western slope to form a deep boundary current.

The polar transition zone corresponds to the boundary between the alpha and beta zones. In our experiments, the transition zone is very narrow and it matches the position where the surface buoyancy flux changes sign, becoming positive toward the north. The surface buoyancy flux changes sign when the negative heat flux becomes overridden by the positive freshwater flux. Importantly, this inversion is not driven by an intensification of the freshwater flux, but rather by the dropping value of the TEC associated with decreasing surface temperatures. If the TEC value is increased at low temperature in the model, the relative effect of salinity on the stratification is decreased and the convective zone is shifted poleward. In the extreme case where the TEC value is made very large for low temperatures (e.g., for a linear EOS with a value of the TEC close to the ocean average value of 2×10^{-4} °C^{-1}), the freshwater flux cannot overcome the large buoyancy loss due to heat fluxes anywhere. The result is a disappearance of the beta ocean in those simulations (not shown). In this study, the wind forcing has been kept unchanged. The large migration of the polar transition zone despite constant wind demonstrates that it is the buoyancy forcing that controls its position rather than the wind. However, the wind forcing can modify the buoyancy forcing through generation of meridional Ekman fluxes and by modulating the strength and structure of basin-scale gyres, indirectly affecting the position of the polar transition. We leave the task of assessing how the wind forcing affects the polar transition for a future work.

There are of course important limitations due to the nature of the single hemisphere basin configuration used in this study. The absence of a reentrant channel complicates the analogy with the Southern Ocean, although it is widely recognized that the general stratification depends critically on the presence of the Southern Ocean to produce a deep reaching circumpolar current and deepen the permanent pycnocline (Gnanadesikan 1999; Wolfe and Cessi 2011). The coarse

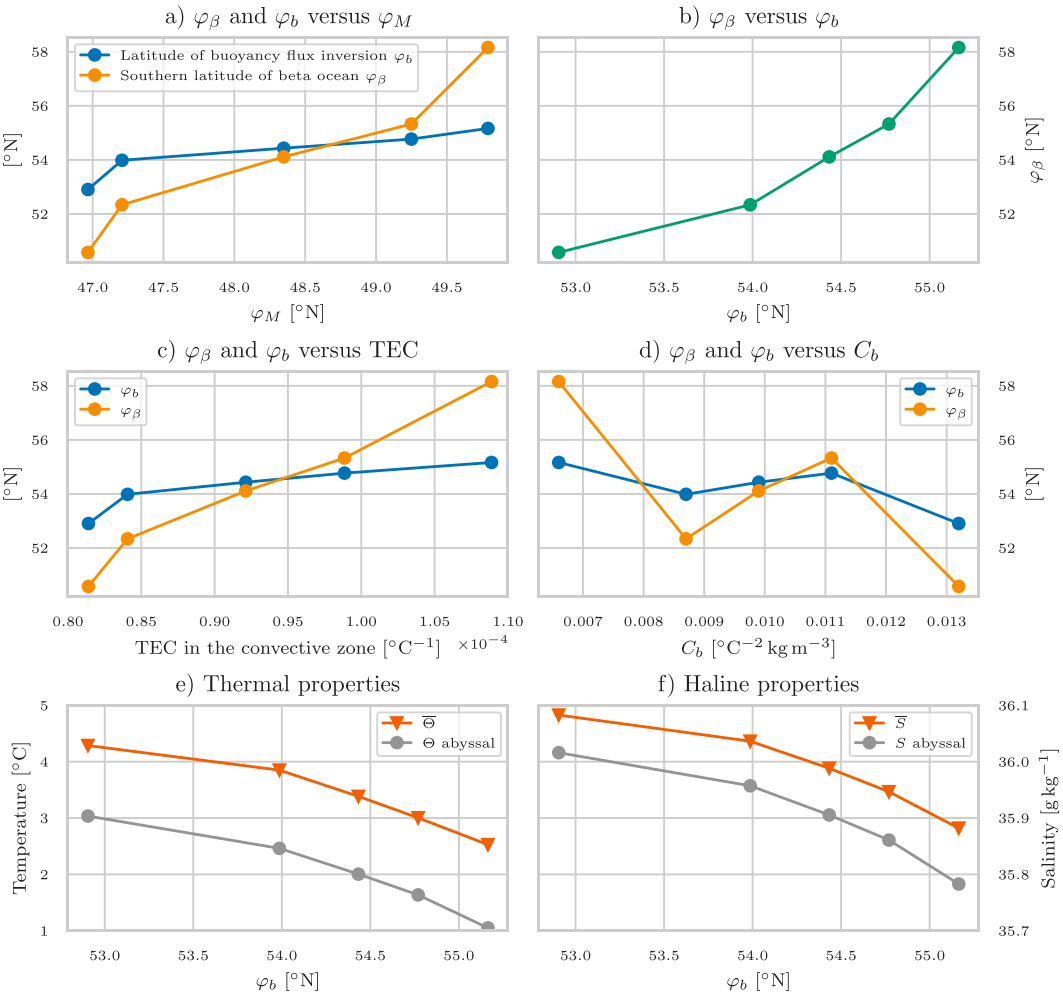

FIG. 10. (a) Latitude of the southern boundary of the beta ocean φ_β and latitude of the buoyancy front φ_b vs φ_M the latitude of maximum σ_0^*, (b) φ_β vs φ_b, (c) φ_b function of the value of the TEC in the convective area, (d) φ_β and φ_b vs cabbeling parameter C_b. Evolution of the basin average and abyssal (e) temperature and (f) salinity as a function of the front latitude. The abyssal properties are computed as latitude–longitude averages over the bottom cell of the ocean.

resolution used here also means mesoscale variability is not explicitly resolved, which would otherwise significantly complicate the structure and variability of the transition zone. As sea ice and brine rejection are not represented in the present idealized model, convection does not occur in the beta region resulting in the absence of a bottom stratification between deep and bottom waters. Sea ice modifies the freshwater forcing, through brine rejection or melting, modulating air–sea fluxes in the polar region. If the added freshwater is transported away from the sea ice formation area, e.g., by Ekman transport, the polar transition may consequently be shifted equatorward and convection in the transition zone may become hindered. Investigation would be needed to determine the contribution of sea ice melting to the freshwater budget around the transition zones. However, our results depend mainly on fluxes into the sea, so we expect the role of TEC variations on the surface buoyancy fluxes to be a robust feature directly applicable to the real ocean. As the transition zone in all basins is characterized by rapid changes in the type of stratification control (Pollard et al. 2002; Carmack 2007; Pauthenet et al. 2019), it is likely that the position of these fronts will remain primarily influenced by the surface buoyancy fluxes.

The mean ocean temperature, through its associated influence on the TEC value, is known to have an impact on the overturning circulation by the induced change of stratification (e.g., de Boer et al. 2007; Schloesser 2020). What has been less discussed is the potential migration of the deep-water formation area. As TEC is primarily a function of surface temperature (Roquet et al. 2015), a change of the TEC driven by surface warming will also impact the relative influence of the heat and freshwater fluxes. This change can be expected to influence in return the global circulation and the deep ocean thermohaline properties. We did not find

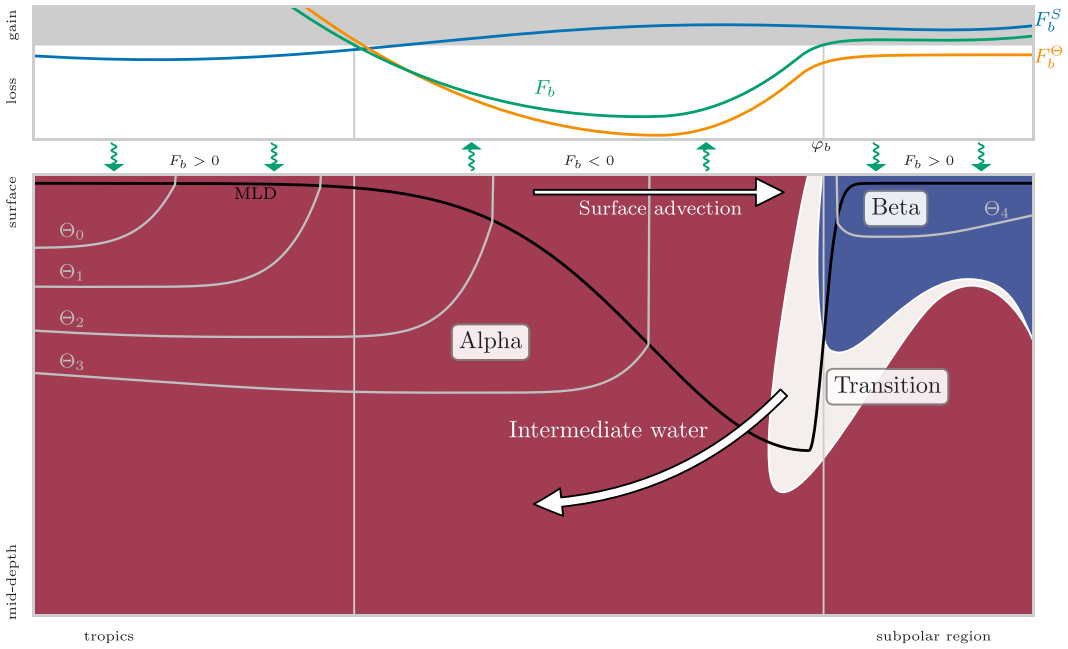

FIG. 11. Zonal conceptual view of the ocean. (top) The surface buoyancy fluxes, where the gray background is for positive fluxes and the white one for negative fluxes. The green wavy arrows represent the surface buoyancy flux: they are oriented downward for buoyancy gain, and upward for buoyancy loss. The two latitudes of buoyancy flux inversion are indicated by the vertical gray lines. (bottom) The zonal view of the ocean is shown. The red color is used for the alpha ocean, blue color for the beta ocean, and white for the transition zone. The mixed layer depth is represented by the black line, and the five gray lines represent five isotherms named by Θ_n with n between 0 and 5.

any indication that the cabbeling effect may be of leading order in setting the position of the polar transition and convective area, as similar locations and structures of the polar transition zone were found for model runs with vastly different cabbeling parameters but similar TEC in the polar area (runs not shown, C_b varying between 0 and 35×10^{-3} °C^{-2} kg m^{-3}). This does not mean, of course, that cabbeling has no effect in the transition zone, as it has been estimated that a significant densification of water masses is generated by cabbeling in transition zones (e.g., Groeskamp et al. 2016); however, this implies that the position and overall structure of the transition zone is probably not determined by the cabbeling effect.

This study highlights the primary importance of surface buoyancy fluxes in setting the general structure of the ocean stratification and the associated meridional overturning. It also documents one key way the thermodynamic properties of seawater have a global impact on the ocean circulation, namely, through the effect of geographic variations of the TEC on the distribution and sign of the surface buoyancy fluxes.

Acknowledgments. The computations were enabled by resources provided by the Swedish National Infrastructure for Computing (SNIC) at Tetralith partially funded by the Swedish Research Council through Grant Agreement 2018-05973. The authors appreciate the helpful reviews from two anonymous reviewers.

Data availability statement. The model data (output) can be found on Zenodo: https://doi.org/10.5281/zenodo.5607673. The scripts for the analyzes are hosted on GitHub, along with the model configuration source files: https://doi.org/10.5281/zenodo.6340730. All the runs and the analyze are reproducible within a few steps.

APPENDIX A

Comparison of MLD

Figure A1 compares the MLD for the five runs, along with the position of the beta ocean boundary. As expected, the beta ocean has a shallow ML, and the deepest ML are found immediately south of the polar transition zone. A clear correlation between the latitude of the maximum MLD, latitude of φ_M and polar TEC value can be seen, indicating that increasing the value of the TEC at low temperature is accompanied with a poleward migration of the polar transition zone.

APPENDIX B

Equivalent Latitude Calculation

This appendix gives the detail of the equivalent latitude calculation for the buoyancy flux inversion. First the area A of the ocean poleward of 48°N that gains buoyancy is

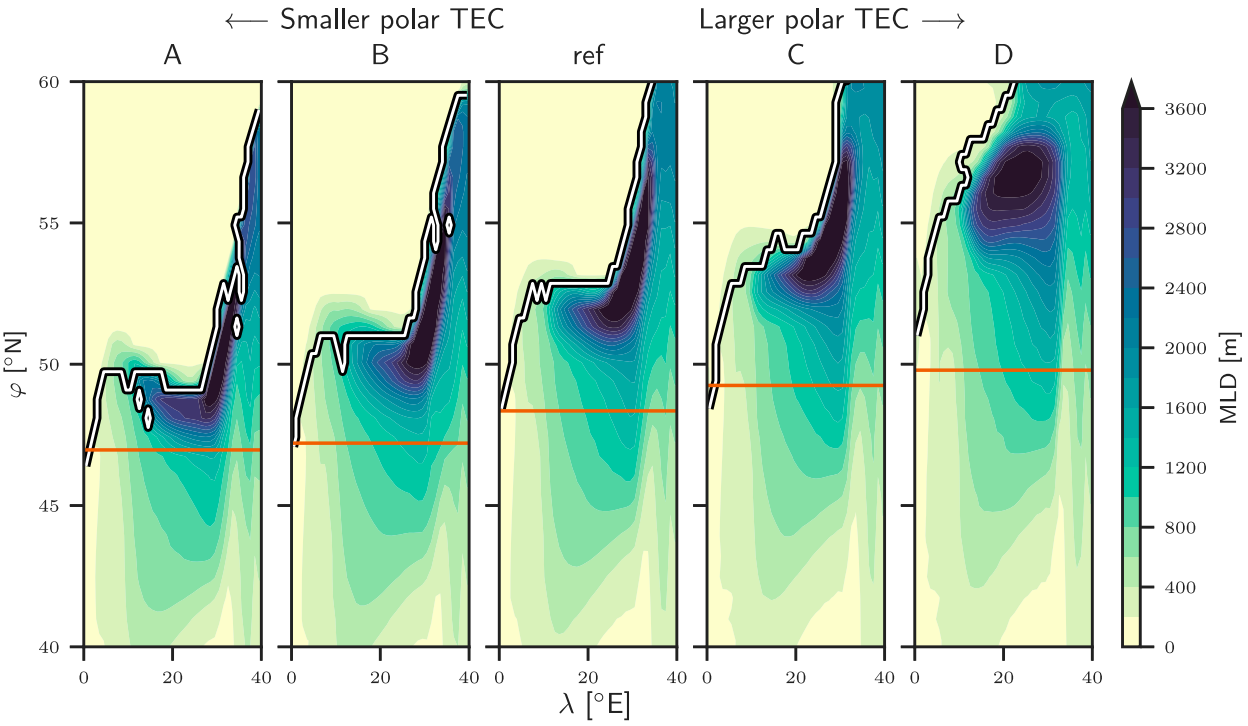

FIG. A1. Annual maximum of MLD for every runs. The white line with black contour represents the −1 value of the SCI under the ML. As the transition zone is very narrow between the alpha and beta oceans, this line corresponds very well to the transition between the alpha and beta oceans. The orange line represents the latitude of φ_M, the latitude of maximum value of σ_0^*.

computed. The area A_{eq} of a zonally uniform ocean bounded by the southern latitude φ_b is calculated as

$$A_{\text{eq}} = A = \int_{\lambda_W}^{\lambda_W} \int_{\varphi_b}^{\varphi_N} a^2 \cos\left(\varphi \frac{\pi}{180}\right) \varphi\lambda, \tag{B1}$$

where $\lambda_W = 0°\text{E}$ ($\lambda_E = 40°\text{E}$) is the western (eastern) coast, $\varphi_N \simeq 60.5°\text{N}$ is the northern boundary of the basin, and $a \simeq 111\,198$ km the length of 1° at the equator. Inverting this equation gives

$$\varphi_b = \arcsin\left[\sin(\varphi_N) - \frac{A}{a^2(\lambda_W - \lambda_E)}\right]. \tag{B2}$$

The same method is used for the area where SCI < -1 to compute the southern boundary of the latitude of the fresh beta area.

REFERENCES

Aagaard, K., and E. C. Carmack, 1989: The role of sea ice and other fresh water in the Arctic circulation. *J. Geophys. Res.*, **94**, 14 485–14 498, https://doi.org/10.1029/JC094iC10p14485.

Bryan, F., 1986: High-latitude salinity effects and interhemispheric thermohaline circulations. *Nature*, **323**, 301–304, https://doi.org/10.1038/323301a0.

Carmack, E. C., 2007: The alpha/beta ocean distinction: A perspective on freshwater fluxes, convection, nutrients and productivity in high-latitude seas. *Deep-Sea Res. II*, **54**, 2578–2598, https://doi.org/10.1016/j.dsr2.2007.08.018.

Cessi, P., 2019: The global overturning circulation. *Annu. Rev. Mar. Sci.*, **11**, 249–270, https://doi.org/10.1146/annurev-marine-010318-095241.

de Boer, A. M., D. M. Sigman, J. R. Toggweiler, and J. L. Russell, 2007: Effect of global ocean temperature change on deep ocean ventilation. *Paleoceanography*, **22**, PA2210, https://doi.org/10.1029/2005PA001242.

de Boyer Montégut, C., 2004: Mixed layer depth over the global ocean: An examination of profile data and a profile-based climatology. *J. Geophys. Res.*, **109**, C12003, https://doi.org/10.1029/2004JC002378.

Garrett, C., and E. Horne, 1978: Frontal circulation due to cabbeling and double diffusion. *J. Geophys. Res.*, **83**, 4651, https://doi.org/10.1029/JC083iC09p04651.

Gent, P. R., and J. C. McWilliams, 1990: Isopycnal mixing in ocean circulation models. *J. Phys. Oceanogr.*, **20**, 150–155, https://doi.org/10.1175/1520-0485(1990)020<0150:IMIOCM>2.0.CO;2.

Gnanadesikan, A., 1999: A simple predictive model for the structure of the oceanic pycnocline. *Science*, **283**, 2077–2079, https://doi.org/10.1126/science.283.5410.2077.

Groeskamp, S., R. P. Abernathey, and A. Klocker, 2016: Water mass transformation by cabbeling and thermobaricity. *Geophys. Res. Lett.*, **43**, 10 835–10 845, https://doi.org/10.1002/2016GL070860.

Hieronymus, M., and J. Nycander, 2013: The buoyancy budget with a nonlinear equation of state. *J. Phys. Oceanogr.*, **43**, 176–186, https://doi.org/10.1175/JPO-D-12-063.1.

Holte, J. W., L. D. Talley, T. K. Chereskin, and B. M. Sloyan, 2012: The role of air-sea fluxes in Subantarctic Mode Water

formation. *J. Geophys. Res.*, **117**, C03040, https://doi.org/10.1029/2011JC007798.

IOC, SCOR, and IAPSO, 2015: The International Thermodynamic Equation of Seawater—2010: Calculation and use of thermodynamic properties. Intergovernmental Oceanographic Commission, Manuals and Guides 56, 220 pp., http://www.teos-10.org/pubs/TEOS-10_Manual.pdf.

Isachsen, P. E., C. Mauritzen, and H. Svendsen, 2007: Dense water formation in the Nordic Seas diagnosed from sea surface buoyancy fluxes. *Deep-Sea Res. I*, **54**, 22–41, https://doi.org/10.1016/j.dsr.2006.09.008.

Iudicone, D., G. Madec, B. Blanke, and S. Speich, 2008: The role of Southern Ocean surface forcings and mixing in the global conveyor. *J. Phys. Oceanogr.*, **38**, 1377–1400, https://doi.org/10.1175/2008JPO3519.1.

Karstensen, J., and D. Quadfasel, 2002: Formation of Southern Hemisphere thermocline waters: Water mass conversion and subduction. *J. Phys. Oceanogr.*, **32**, 3020–3038, https://doi.org/10.1175/1520-0485(2002)032<3020:FOSHTW>2.0.CO;2.

——, and K. Lorbacher, 2011: A practical indicator for surface ocean heat and freshwater buoyancy fluxes and its application to the NCEP reanalysis data. *Tellus*, **63A**, 338–347, https://doi.org/10.1111/j.1600-0870.2011.00510.x.

Klocker, A., and T. J. McDougall, 2010: Influence of the nonlinear equation of state on global estimates of dianeutral advection and diffusion. *J. Phys. Oceanogr.*, **40**, 1690–1709, https://doi.org/10.1175/2010JPO4303.1.

Kuhlbrodt, T., A. Griesel, M. Montoya, A. Levermann, M. Hofmann, and S. Rahmstorf, 2007: On the driving processes of the Atlantic meridional overturning circulation. *Rev. Geophys.*, **45**, RG2001, https://doi.org/10.1029/2004RG000166.

Lazar, A., G. Madec, and P. Delecluse, 1999: The deep interior downwelling, the Veronis effect, and mesoscale tracer transport parameterizations in an OGCM. *J. Phys. Oceanogr.*, **29**, 2945–2961, https://doi.org/10.1175/1520-0485(1999)029<2945:TDIDTV>2.0.CO;2.

Lazier, J. R., 1980: Oceanographic conditions at Ocean Weather Ship Bravo, 1964–1974. *Atmos.–Ocean*, **18**, 227–238, https://doi.org/10.1080/07055900.1980.9649089.

Lévy, M., P. Klein, A.-M. Tréguier, D. Iovino, G. Madec, S. Masson, and K. Takahashi, 2010: Modifications of gyre circulation by sub-mesoscale physics. *Ocean Model.*, **34**, 1–15, https://doi.org/10.1016/j.ocemod.2010.04.001.

Madec, G., and Coauthors, 2019: NEMO ocean engine. Notes du Pôle de modélisation de l'Institut Pierre-Simon Laplace 27, Zenodo, https://doi.org/10.5281/ZENODO.1464816.

Marsh, R., A. J. G. Nurser, A. P. Megann, and A. L. New, 2000: Water mass transformation in the Southern Ocean of a global isopycnal coordinate GCM. *J. Phys. Oceanogr.*, **30**, 1013–1045, https://doi.org/10.1175/1520-0485(2000)030<1013:WMTITS>2.0.CO;2.

Marshall, J. C., R. G. Williams, and A. J. G. Nurser, 1993: Inferring the subduction rate and period over the North Atlantic. *J. Phys. Oceanogr.*, **23**, 1315–1329, https://doi.org/10.1175/1520-0485(1993)023<1315:ITSRAP>2.0.CO;2.

Mauritzen, C., and S. Häkkinen, 1999: On the relationship between dense water formation and the "Meridional Overturning Cell" in the North Atlantic Ocean. *Deep-Sea Res. I*, **46**, 877–894, https://doi.org/10.1016/S0967-0637(98)00094-6.

McCartney, M. S., 1982: The subtropical recirculation of mode-waters. *J. Mar. Res.*, **40**, 64.

McDougall, T. J., 2003: Potential enthalpy: A conservative oceanic variable for evaluating heat content and heat fluxes. *J. Phys. Oceanogr.*, **33**, 945–963, https://doi.org/10.1175/1520-0485(2003)033<0945:PEACOV>2.0.CO;2.

——, and Y. You, 1990: Implications of the nonlinear equation of state for upwelling in the ocean interior. *J. Geophys. Res.*, **95**, 13 263–13 276, https://doi.org/10.1029/JC095iC08p13263.

Nycander, J., M. Hieronymus, and F. Roquet, 2015: The nonlinear equation of state of sea water and the global water mass distribution. *Geophys. Res. Lett.*, **42**, 7714–7721, https://doi.org/10.1002/2015GL065525.

Pauthenet, E., F. Roquet, G. Madec, and D. Nerini, 2017: A linear decomposition of the Southern Ocean thermohaline structure. *J. Phys. Oceanogr.*, **47**, 29–47, https://doi.org/10.1175/JPO-D-16-0083.1.

——, ——, ——, J.-B. Sallée, and D. Nerini, 2019: The thermohaline modes of the global ocean. *J. Phys. Oceanogr.*, **49**, 2535–2552, https://doi.org/10.1175/JPO-D-19-0120.1.

Pedlosky, J., 1996: *Ocean Circulation Theory*. Springer, 467 pp., https://doi.org/10.1007/978-3-662-03204-6.

Petit, T., M. S. Lozier, S. A. Josey, and S. A. Cunningham, 2020: Atlantic deep water formation occurs primarily in the Iceland Basin and Irminger Sea by local buoyancy forcing. *Geophys. Res. Lett.*, **47**, e2020GL091028, https://doi.org/10.1029/2020GL091028.

Piola, A. R., and D. T. Georgi, 1982: Circumpolar properties of Antarctic intermediate water and Subantarctic Mode Water. *Deep-Sea Res.*, **29A**, 687–711, https://doi.org/10.1016/0198-0149(82)90002-4.

Pollard, R., M. Lucas, and J. Read, 2002: Physical controls on biogeochemical zonation in the Southern Ocean. *Deep-Sea Res. II*, **49**, 3289–3305, https://doi.org/10.1016/S0967-0645(02)00084-X.

Roden, G. I., 1970: Aspects of the mid-pacific transition zone. *J. Geophys. Res.*, **75**, 1097–1109, https://doi.org/10.1029/JC075i006p01097.

Rooth, C., 1982: Hydrology and ocean circulation. *Prog. Oceanogr.*, **11**, 131–149, https://doi.org/10.1016/0079-6611(82)90006-4.

Roquet, F., G. Madec, L. Brodeau, and J. Nycander, 2015: Defining a simplified yet "realistic" equation of state for seawater. *J. Phys. Oceanogr.*, **45**, 2564–2579, https://doi.org/10.1175/JPO-D-15-0080.1.

Ruddick, B., 1983: A practical indicator of the stability of the water column to double-diffusive activity. *Deep-Sea Res.*, **30A**, 1105–1107, https://doi.org/10.1016/0198-0149(83)90063-8.

Sallée, J.-B., K. Speer, S. Rintoul, and S. Wijffels, 2010: Southern Ocean thermocline ventilation. *J. Phys. Oceanogr.*, **40**, 509–529, https://doi.org/10.1175/2009JPO4291.1.

Schloesser, F., 2020: The Atlantic meridional overturning circulation and the cabbeling effect. *J. Phys. Oceanogr.*, **50**, 2561–2572, https://doi.org/10.1175/JPO-D-20-0085.1.

Schmitt, R. W., P. S. Bogden, and C. E. Dorman, 1989: Evaporation minus precipitation and density fluxes for the North Atlantic. *J. Phys. Oceanogr.*, **19**, 1208–1221, https://doi.org/10.1175/1520-0485(1989)019<1208:EMPADF>2.0.CO;2.

Sloyan, B. M., and S. R. Rintoul, 2001: Circulation, renewal, and modification of Antarctic mode and intermediate water. *J. Phys. Oceanogr.*, **31**, 1005–1030, https://doi.org/10.1175/1520-0485(2001)031<1005:CRAMOA>2.0.CO;2.

Speer, K., S. R. Rintoul, and B. Sloyan, 2000: The diabatic Deacon cell. *J. Phys. Oceanogr.*, **30**, 3212–3222, https://doi.org/10.1175/1520-0485(2000)030<3212:TDDC>2.0.CO;2.

Speer, K. G., H.-J. Isemer, and A. Biastoch, 1995: Water mass formation from revised COADS data. *J. Phys. Oceanogr.*, **25**, 2444–2457, https://doi.org/10.1175/1520-0485(1995)025<2444:WMFFRC>2.0.CO;2.

Stewart, K. D., and T. W. N. Haine, 2016: Thermobaricity in the transition zones between alpha and beta oceans. *J. Phys. Oceanogr.*, **46**, 1805–1821, https://doi.org/10.1175/JPO-D-16-0017.1.

Thomas, L. N., and C. J. Shakespeare, 2015: A new mechanism for mode water formation involving cabbeling and frontogenetic strain at thermohaline fronts. *J. Phys. Oceanogr.*, **45**, 2444–2456, https://doi.org/10.1175/JPO-D-15-0007.1.

Walin, G., 1982: On the relation between sea-surface heat flow and thermal circulation in the ocean. *Tellus*, **34**, 187–195, https://doi.org/10.3402/tellusa.v34i2.10801.

Wolfe, C. L., and P. Cessi, 2011: The adiabatic pole-to-pole overturning circulation. *J. Phys. Oceanogr.*, **41**, 1795–1810, https://doi.org/10.1175/2011JPO4570.1.

——, and ——, 2014: Salt feedback in the adiabatic overturning circulation. *J. Phys. Oceanogr.*, **44**, 1175–1194, https://doi.org/10.1175/JPO-D-13-0154.1.

Woods, J. D., 1985: The physics of thermocline ventilation. *Coupled Ocean-Atmosphere Modelling*, J. C. J. Nihoul, Ed., Elsevier Oceanography Series, Vol. 40, Elsevier, 543–590, https://doi.org/10.1016/S0422-9894(08)70730-X.